Analysis of Exponential Frequency Diverse Array for Short-Range Beam Focusing Technology

Woohyeok Choi, Apostolos Georgiadis, *Fellow*, *IEEE*, Manos M. Tentzeris, *Fellow*, *IEEE*, and Sangkil Kim, *Senior Member*, *IEEE*

***Abstract*—The frequency diverse array (FDA) is a promising technology because of its angle-range-dependent beam pattern. The FDA has unique properties, such as beam scanning and focusing, which are difficult to achieve using the conventional phased antenna array theory. In this study, the relationship between range and frequency increment is analyzed, and the fundamental operation principle of FDA is thoroughly investigated. The effect of coupling among antenna elements is also discussed to analyze the FDA theory. Further, a novel exponential FDA method for short-range beam focusing is presented based on the proposed FDA analysis method. The proposed method has been investigated through various case studies and applied to research efforts on FDA methods. The FDA design procedures and analysis methods are also presented in this paper.**

***Index Terms*—Exponentially increasing frequency increment, frequency diverse array (FDA), periodicity, quasi-pulse wave, standard deviation of frequency increment (SDFI), wireless power transfer (WPT).**

I. Introduction

The Frequency Diverse Array (FDA) technique reported in [1]-[3] has several novel properties, such as auto-scanning [1] and dot-shaped [4]-[6] beam patterns, which are different from conventional phased arrays. The time-invariant FDA was also reported in [7]-[9]. The key design parameters of the FDA, such as wave propagation property ($r = t \cdot c$), time (t), frequency increment (Δf_m), and phase (φ), should be thoroughly analyzed to achieve the desired beam patterns. The reported research efforts in [4], [10]-[12] proposed the application of time delay and periodicity to analyze and design FDA system. Linear FDA is a well-known method comprising of auto-beam scanning properties, as compared to other methods that focus on electromagnetic (EM) energy in a one spot. Nonlinearly [13], [14] or randomly [15], [16] changing frequency FDA methods have been proposed to focus EM energy on a single spot in a given range.

A short-range FDA is proposed in [8], [17] to define FDA for all ranges. The reported short-range FDA methods focus on EM energy at distances within several meters using a short pulse. In [4], an FDA with a 2D circular antenna array was proposed to clarify the relationship between time and range. This work demonstrated periodically focused beams in range. However, non-periodic cases are not presented. In recent years, the FDA system has been applied in many fields, such as secure communication [18], [19] and wireless power transfer (WPT) [20], owing to its novel angle-range-dependent beam-pattern property.

In this paper, a novel FDA method to focus EM energy for short-range applications using continuous waves (CWs) has been proposed. This study aims to eliminate ambiguity related to range and time to apply the concept of the FDA in real. A thorough analysis of the phase offset based on the meaning of time in the FDA is also presented based on computational data. Further, the relationship among the frequency increment step (Δf_m), time (t), and range (R) was studied rigorously. The FDA is classified into two cases based on its beam pattern: 1) periodic and 2) non-periodic FDAs. The phase offset value was examined by comparing those two cases. Reported FDA methods, including exponentially increasing frequency increments, are illustrated based on the concepts and definitions discussed in this paper. For a practical approach, the effect of coupling among the antenna elements for the FDA is analyzed. As a case study, a WPT system using FDA was designed, and its performance is discussed in this paper.

The remainder of this paper is organized as follows. In Section II, the conventional FDA methods are briefly reviewed and analyzed. In Section III, a rigorous analysis of the time parameter is discussed to clarify its function in FDA theory. The definition and analysis of time presented in this study is applicable to all cases of FDA methods, such as linear frequency, nonlinearly changing frequency, and random frequency FDAs. A novel method for analyzing arbitrarily defined FDA method is also presented. In Section IV, two methods of FDA are introduced. The proposed FDA analysis method is validated, and a case study of the proposed FDA is presented in Section V.

This work was supported in part by the Korea government (MSIT) through the National Research Foundation of Korea (NRF) under Grant 2020R1C1C1003362. (*Corresponding author: Sangkil Kim*)

W. Choi and S. Kim are with the Department of Electronics Engineering, Pusan National University, Busan, Republic of Korea (e-mail: ksangkil3@pusan.ac.kr).

A. Georgiadis is with the School of Engineering and Physical Sciences, Herriot-Watt University, Edinburgh, UK.

M. M. Tentzeris is with the School of Electrical and Computer Engineering, Georgia Institute of Technology, Atlanta, GA 30318 USA.

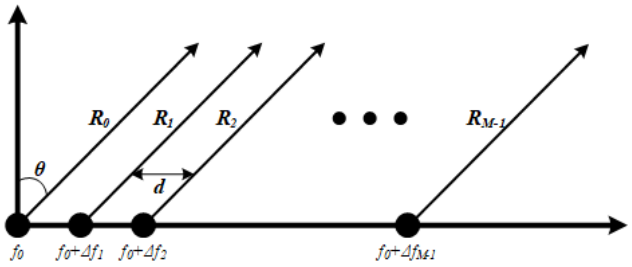

Fig. 1. Configuration of ULA FDA

II. Analysis of Conventional FDA Method

The uniform linear array (ULA) FDA, which consists of M elements and inter-element spacing, d, is illustrated in Fig. 1. The frequency of the signal fed to the m-th antenna element is

$$f_m = f_0 + \Delta f_m, \qquad m = 1, \cdots, (M-1) \tag{1}$$

where f_0 is the reference frequency and Δf_m is the frequency increment. At the reference position (R, θ) (where R is the range in meters and θ is the azimuth angle in degrees), the overall signal, $S(t, R, \theta)$, at time, t, is

$$S(t,R,\theta) = \sum_{m=0}^{M-1} s_m\left(t - \frac{R_m}{c}\right) = \sum_{m=0}^{M-1} e^{j\left(2\pi \int_0^{t-\frac{Rm}{c}} f_m(t)dt + \varphi_m\right)} \tag{2}$$

where φ_m is the phase offset of the m-th element, c is the speed of light, s_m is the signal at the m-th antenna element, and R_m is the distance between the m-th antenna element and the reference position where $R_m \approx R - md\sin\theta$ [21]. The phase term in (2) is written in integral form because of the relationship between the frequency and phase [10]. It can be re-written as (3), if f_m is not a function of time, t.

$$S(t,R,\theta) = \sum_{m=0}^{M-1} e^{j\left[2\pi f_m\left(t - \frac{R - md\sin\theta}{c}\right) + \varphi_m\right]} \tag{3}$$

Array factor (AF) can be expressed as (4) by eliminating the terms unrelated to array number, m, from (3), when $f_0 \gg \Delta f_m$.

$$\mathrm{AF}(t,R,\theta) \approx \sum_{m=0}^{M-1} e^{j[\varphi_m^{RTF} + \varphi_m^{AE} + \varphi_m]} = \sum_{m=0}^{M-1} e^{j\varphi_m^{AF}} \tag{4}$$

d is set to (5) to suppress grating lobes based on the array theory

$$d \le \frac{\lambda_{max}}{2} \tag{5}$$

where λ_{max} is the wavelength at the lowest frequency. Equation (4) is the basic form of the FDA. It consists of two phase terms: range-time-frequency and angle-element terms. The range-time-frequency term (φ_m^{RTF}) is

$$\varphi_m^{RTF} = 2\pi\Delta f_m\left(t - \frac{R}{c}\right) \tag{6}$$

The angle-element term (φ_m^{AE}) is

$$\varphi_m^{AE} = \frac{2\pi f_0 md\sin\theta}{c} \tag{7}$$

Other FDA methods can be easily derived and analyzed from (4)–(7). The simplest method of the FDA is using linearly increasing frequency increments. The frequency increment is expressed as follows:

$$\Delta f_m = m\Delta f \tag{8}$$

In this case, the AF expressed in (4) is written as

$$AF(t,R,\theta) = \sum_{m=0}^{M-1} e^{j2\pi m\left[\Delta f\left(t - \frac{R}{c}\right) + \frac{2\pi f_0 d\sin\theta}{c}\right]} \tag{9}$$

when $\varphi_m = 0$. In (9), both φ_m^{RTF} and φ_m^{AE} are proportional to m. The linearly increasing frequency step results in maximum E-field (focused beam) points for all ranges and different angles, resulting in time-variant beam scanning properties [1].

The log-FDA method is proposed to produce a single maximum point in an angle-range-dependent beam pattern [13]. The frequency increment of the log-FDA is expressed as

$$\Delta f_m = \log(m+1)\,\delta \tag{10}$$

The offset parameter δ is an arbitrary number to optimize beam patterns. The AF of the log-FDA is derived as follows:

$$AF(t,R,\theta) = \sum_{m=0}^{M-1} e^{j\left[2\pi\log(m+1)\delta\left(t - \frac{R}{c}\right) + \frac{2\pi f_0 md\sin\theta}{c} + \varphi_m\right]} \tag{11}$$

Creating a single focusing point in angle-range-dependent beam patterns is challenging for the log-FDA when the phase offset is zero. Thus, a non-zero offset phase term, φ_m, is proposed to focus on the electromagnetic (EM) energy at a desired position as expressed in (12).

$$\varphi_m = \frac{2\pi\log(m+1)\delta R_0}{c} - \frac{2\pi f_0 md\sin\theta_0}{c} \tag{12}$$

The AF of the log-FDA is modified as

$$AF(t,R,\theta) = \sum_{m=0}^{M-1} e^{j\left[2\pi\delta\log(m+1)\left(t - \frac{R-R_0}{c}\right) + \frac{2\pi f_0 md(\sin\theta - \sin\theta_0)}{c}\right]} \tag{13}$$

The AF expressed in (13) creates a single maximum point in the angle-range-dependent beam pattern at (R_0, θ_0) because the frequency increment has a nonlinear increase rate (φ_m^{RTF} and φ_m^{AE} are not proportional to m). The difference between the rate of frequency increment, consequently, leads to a difference between φ_m^{RTF} and φ_m^{AE}. This results in a phase difference among the antenna elements, resulting in a single maximum point in the beam pattern (non-periodic beam pattern). The log-FDA method features a single maximum point and ease of modification as compared to the linearly increasing method reported in [6], [15], [22].

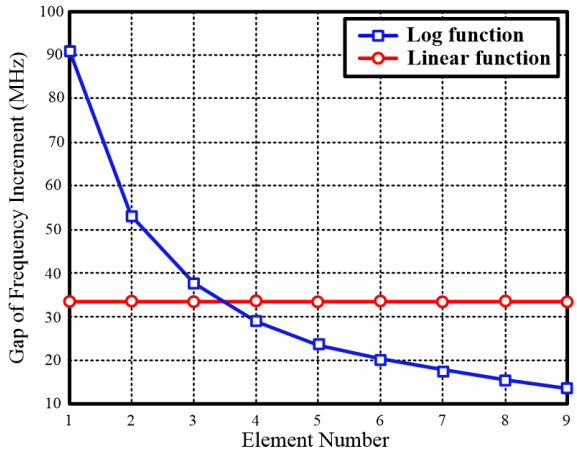

Fig. 2. Frequency increment of log function and linear function. Both cases have the same maximum frequency increment of value 300 MHz.

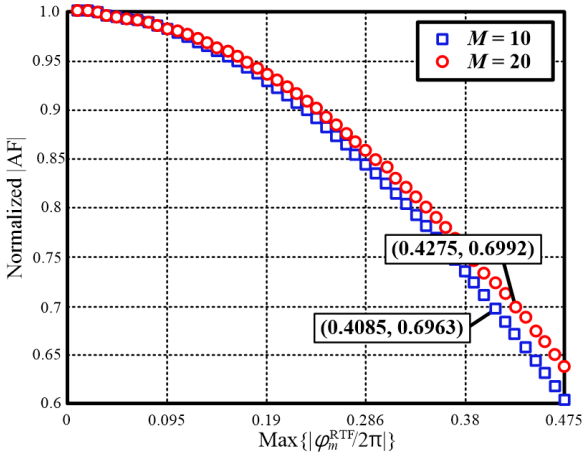

Fig. 3. Normalized AF of a linear frequency increment method with different M, where $\theta = 0°$, and $t = 0s$.

III. Frequency Increment and AF

The relationship between time (t) and range (R) was analyzed in [10]. The correlation between the frequency increment (Δf_m) and time (t), which are critical parameters of AF, has not been clearly reported thus far. In this section, the relationship between the AF and the frequency increment is thoroughly analyzed.

A. Range (R) and Frequency Increment (Δf_m)

The frequency increment (Δf_m) is multiplied by the range (R) and time (t) in the phase term (φ_m^{AF}) of AF, as expressed in (4). When t = 0 and $d = \lambda_{max}/2$, φ_m^{AF} in (4) is reduced to

$$\varphi_m^{AF} = 2\pi\left[-\frac{\Delta f_m R}{c} + \frac{m\sin\theta}{2}\right] \tag{14}$$

where the phase offset is zero ($\varphi_m = 0$). Equation (14) can be divided into two parts: range-frequency (φ_m^{RF}) and angle-element (φ_m^{AE}) terms. These terms are expressed in (15) and (16), respectively.

$$\varphi_m^{RF} = -2\pi\frac{\Delta f_m R}{c} \tag{15}$$

$$\varphi_m^{AE} = m\pi\sin\theta \tag{16}$$

The magnitude of φ_m^{AE} is less than or equal to $m\pi$ because $|\sin\theta| \leq 1$. This implies that the phase of the AF for the FDA can be manipulated when $\sin\theta$ is not 0. The FDA method cannot make a beam pattern with multiple maximum points, without a range-frequency product term unless $\sin\theta$ is equal to 0, because of the property of the exponential function. The sum of several exponential functions has a maximum value when all the phase terms are $2\cdot(N-1)\cdot\pi$, where N is an integer.

The φ_m^{RF} term should have a proper value to create an angle-range-dependent beam pattern. In this section, the frequency increment method is investigated to analyze the φ_m^{RF} factor. First, it is worth examining how the FDA forms an angle-range-dependent beam pattern. The FDA employs multiple antenna radiating signals at different frequencies, resulting in different phases. In (14), the frequency increment (Δf_m) between adjacent elements is clearly an important parameter for the angle-range-dependent property. Fig. 2 shows the difference between the frequency increments of the two methods: linear and log FDA methods. It also shows why the linear frequency increment FDA makes the beam scanning property. A linear frequency increment step results in the beam scanning property because (14) is canceled out. The nonlinear increase in the frequency increment of the log-FDA results in a non-zero value of (14), and it has a non-scanning beam pattern. The method of identifying the scanning property of FDA is deeply related to time, and it is discussed in next section.

To eliminate the ambiguity of the range, the $\varphi_m^{RTF}/2\pi$ value (Fig. 3) of 0.4085 was chosen as a design example of an angle-range-dependent beam pattern. The number of dots is 50 and 43rd dot is selected where the maximum value shown in Fig. 3 is 0.475. Its calculated $\varphi_m^{RTF}/2\pi$ value is 0.4085. The value of 0.475 is discretized in 50 points to show the change of FDA within 3% error. The 43rd point is a first point which makes the FDA system have half power 7.07 calculated as $\mathrm{Max}(AF)/\sqrt{2}$ (Fig. 3). It represents the minimum value of $\varphi_m^{RTF}/2\pi$ which makes the FDA system have half power. This can be translated to a reasonable difference of 0.045 derived by $0.4085/(M-1)$, where M = 10 in linear FDA case. A difference less than 0.045 makes the phased array property, rather than operating as the FDA. This example shows the relationship between the range (R) and frequency increment. A large frequency step is required to focus the electromagnetic energy at a relatively short distance from the source. For example, the required frequency difference between adjacent antenna elements is larger than 1.35 kHz when the desired beam focusing range is 10 km from the FDA antenna system. However, the required frequency difference was larger than 135 kHz when the target range is 100 m.

The sign of the frequency increment is important because it affects the beam pattern. The co-existence of both the increasing and decreasing frequency steps shows a dot-shaped beam pattern. The shape of the increasing or decreasing frequency step has crescent-like beam patterns in the angle-range coordinate. For example, if an FDA has a monotonically

increasing frequency step, the last antenna element radiates the highest frequency signal. In this case, φ_m^{AE} term should be increased to compensate for the decreasing φ_m^{RF}, according to (13). This results in a crescent-like beam pattern. The case of monotonically decreasing frequency steps can also be explained in the same manner. The co-existence of increasing and decreasing frequency steps generates a dot-shaped beam pattern, which is discussed in Section V.

The maximum of frequency increment also affected the beam pattern. For example, two FDAs have the same frequency increment method, but different maximum frequency increment. Previously, it was found that the frequency increment rate was related to range coverage. A larger range-frequency term (φ_m^{RF}) is more sensitive to the range term (R) because it affects the AF phase. When the range coverage needs to be manipulated, a larger range-frequency term is required to have a larger maximum frequency. This suggests that any range coverage can be obtained by the FDA. When choosing frequency increment, two properties should be considered: 1) $f_0 \gg \Delta f_m$, 2) $\Delta f_m \leq \pi \cdot c/[2 \cdot (M-1) \cdot d]$ [2].

B. Time (t), Frequency Increment (Δf_m), and Range (R)

All the design parameters of the FDA, such as time (t), range (R), and frequency increment (Δf_m), are closely related to each other. The relationship between the frequency increment and time is analyzed in this section. A notable difference between linearly increasing frequency increments and nonlinearly changing ones is the number of AF peaks in the given range. It should be noted that the number of AF maximum points and their periods are the functions of range and frequency increments. For the linearly increasing frequency step, the period of peaks is a function of $1/\Delta f$, as reported in [12]. The most popular frequency increment scheme in the FDA is using a nonlinearly changing frequency increment owing to its single maximum property of the AF in a given range. Thus, a new analysis method is required to thoroughly understand the periodicity of the nonlinearly increasing FDA.

Finding the periodicity of the AF intuitively is challenging and important. The FDA systems can be divided into scanning FDA and non-scanning depending on whether or not they are periodic. Periodicity by time occurs when a dot product of time and frequency increment ($t \cdot \Delta f_m$) is an integer number, according to (4). In this study, the greatest common divisor (GCD) of the frequency increment is calculated to analyze the periodicity of nonlinear frequency increment cases. Zero value and a sign of the frequency increment were both not considered because of the nature of the GCD. For nonlinear frequency increment cases, if GCD exists, every frequency increment can be expressed as an integer multiplied by the GCD. The proposed method of GCD value calculation helps to understand and analyze FDA methods. The period ($T_{non\text{-}linear}$) of this FDA is written as

$$T_{non-linear} = \frac{1}{n_{non-linear}} \tag{17}$$

where the smallest frequency increment is $\mathrm{GCD} \cdot n_{non-linear}$ (where nonlinear is an integer number). This principle is true, except that a nonlinearly changing frequency step is an integer number because it is the same case as the linear FDA. Using (17), it is possible to explain why the nonlinear frequency increase has a single maximum point in a given range. The FDA does not have periodicity when the difference in frequency increments has a purely theoretical infinite decimal number. This indicates that the AF has a periodicity when the frequency increment does not have an infinite decimal or GCD. This is proved by the relationship between the time and frequency increment. If a frequency increment is not an infinite decimal number, it can be corrected to an integer by multiplying the time term.

Using the relationship between the frequency increment, range, and time, frequency increment methods for focusing EM energy at other desired locations, (R_l, θ_l), can be defined, where l is the number of other locations. The condition for making other maximum points is

$$\varphi_m^{RF} + \varphi_m^{AE} = \varphi_{min}^{AF} + 2N\pi \tag{18}$$

where φ_{min}^{AF} is the minimum value of φ_m^{AF}. The other maximum points, (R_l, θ_l), can be calculated by using (18). Detailed calculation method is discussed in Section IV.

The role of the phase offset (φ_m) is investigated in terms of time (t) to clarify the definition of φ_m in the FDA. In (12), the phase offset can be separated into two parts: the range-time-frequency and angle-element terms. The phase offset related to the angle-element term was used to set the maximum point in the aiming angle. The phase offset related to the range-time-frequency term is used to set the maximum point in the aiming range. However, this property does not set the maximum point in the aiming range when time is zero, because this term indicates time delay. Thus, the accurate relationship between the time and range should be analyzed.

In (6), the relationships between range, frequency, and time are presented. Equation (4) shows that the time term is related to the phase term. Based on these observations, $t = 0$ indicates that the phase of all antenna elements is zero. This principle is true only if the phase excitation is zero. To make a single maximum point, $c \cdot T$ should be considered using a nonlinear frequency increment, where T is the period of the FDA beam pattern.

Clearly, the range in the phase offset (φ_m) of AF is time delay. When $\varphi_m = 2\pi\Delta f_m R_0/c$, the time at which the maximum point in R is expressed as

$$t = T + T_1 = T + \frac{R - R_0}{c} \tag{19}$$

Equation (19) provides an indication that making accurate time expressions is difficult for existing angle-range-dependent beam patterns when the frequency increment is an infinite decimal number (e.g., logarithmically increasing frequency step). This is because the phase values of all antennas are $2 \cdot (N-1) \cdot \pi$ or the same phase, when the frequency increment is an infinite decimal number. In addition to this, the AF is not a periodic function of time when the frequency increment step is

an infinite decimal number. For instance, the time (T_1) at which the maximum point at R has a negative value ($T_1 = (R-R_0)/c < 0$) when FDA method does not have periodicity and R_0 is a positive value ($R_0 > 0$).

In this study, two methods are used to analyze the FDA in angle-range coordinate planes: 1) manipulation of phase offset and 2) round-up/-down of the frequency increment step. For the manipulation of the phase offset, t should be zero to the focus beam at R_0, when T is not applicable according to (19). The phase offset should be manipulated to create a symmetric focused beam pattern at R with a nonperiodic frequency increment. For example, (12) can be modified as follows:

$$\varphi_m = -\left(\frac{2\pi \log(m+1)\delta R_0}{c} + \frac{2\pi f_0 md \sin\theta_0}{c}\right) \tag{20}$$

The main idea is to change the sign of the original φ_m positive value to modify the time when the maximum point is formed at a specific position. The sign of φ_m is changed because of new property of phase offset found in previous section. The time at which the maximum point at (R, θ_0) is derived as (21) when the AF in (11) is not a period function of time is given by

$$t = \frac{R + R_0}{c} \tag{21}$$

Phase offsets introduce special properties of the FDA when using (21). The time when the focused beam arrives at the desired position can be adjusted. This is a different point compared to a phased array [23], [24].

The round-up/-down of the frequency increment step provides periodicity to all FDA methods. This can be understood using the GCD property. This method makes every frequency step an integer, and every frequency step has a period of $1/n_{non-linear}$.

Equations (17), (19), and (21) help find the exact angle-range-dependent beam pattern with respect to time, as discussed in Section II. The relationships among time, range, and frequency increments were investigated. It is worth investigating the meaning of time based on the frequency increment and range. It is shown that a large maximum frequency increment step makes the angle-range-dependent beam pattern more focused in terms of range because of the multiplicative relationship between range and frequency increment. In other words, FDA, which has a large frequency increment step, has a shorter duration in terms of time. This idea is easily adopted by the equation $t = r/c$, which implies that a small range coverage makes a short time duration. The range coverage is small when a short pulsed wave is radiated by the array antenna.

Based on all the design parameters of the FDA, a new quasi-pulse wave of FDA is presented. In this section, the relationship between time and range coverage is analyzed. The relationship between the frequency increment and range coverage is also studied here. Both the short pulse duration and large frequency step of CW make up the short-range coverage.

C. FDA Analysis Methods

A difference in the frequency increment shows the relationship between the range (R) and frequency increment (Δf_m). To analyze the AF more easily, a standard deviation of the frequency increment (SDFI) method is proposed. The sum of the frequency step differences is expressed as

$$\Delta f_m^{dif} = \sum_{m=0}^{M-2} (\Delta f_{m+1} - \Delta f_m) \tag{22}$$

The Δf_m^{ndif} is defined as (23)

$$\Delta f_m^{ndif} = \begin{cases} \Delta f_m^{dif}, & \Delta f_m^{dif} \geq \Delta f_{min}^{dif} \\ 0, & \Delta f_m^{dif} < \Delta f_{min}^{dif} \end{cases} \tag{23}$$

where Δf_{min}^{dif} is 0.045 when $M = 10$. Then, SDFI value is defined as

$$\text{SDFI} = \frac{\sqrt{\frac{\sum_{m=0}^{M_D-2}\left(\Delta f_m^{ndif} - \Delta f_{mean}^{ndif}\right)^2}{M_D - 1}} \times R_G,}{\text{c}} \tag{24}$$

where R_G is the focused range from (20), M_D from (23) is the number of Δf_m^{ndif}, and Δf_{mean}^{ndif} is the mean value of Δf_m^{ndif}. The proposed SDFI method is valid when one of these conditions is met: 1) the same value of difference between the minimum and maximum values of the frequency increment and 2) the same frequency increment method.

The proposed SDFI has two notable cases. An antenna array has a scanning property when the SDFI value is 0. It occurs when all frequency increments are the same (uniform FDA) or in the case of a phased array. The difference between the uniform FDA and phased array results from M_D. In the beam scanning case, $M_D = M - 1$ was true. However, in the phased array case, $M_D \neq M - 1$ because the difference in frequency increments is neglected due to (23). Hence, the smaller M_D is, the closer beampattern is to phased array case. Only using M_D, the approximate pattern of FDA could be predicted. The shape of an EM energy-focused spot can be predicted using the proposed SDFI method. If the SDFI value is large, the beam pattern appears similar to a circular full moon-shaped dot, as discussed in Section V. In addition to this, FDA method which has lower SDFI value represents tendency to have lower density of maximum point. Conversely, the larger case of SDFI shows tendency to have larger.

The number of antenna elements (M) should be the same to apply the proposed SDFI method to compare the FDA methods. For example, Fig. 3 shows the maximum absolute value of φ_m^{RTF}, when $M = 20$ if $\varphi_m^{RTF}/2\pi$ is a linear function of M. Different M value has an effect on the maximum value of (0.4275 calculated as $0.475 \cdot 45/50$ when M = 20) and Δ (0.0225 as $0.4275/(M-1)$). It has different value compared with the maximum value illustrated when M = *10*. By

comparing the SDFI values of FDA methods, the figure of the maximum point and the overall beam pattern in one period time can be estimated by M_D and the value of SDFI.

IV. Exponentially Increasing Frequency Increment

There are few FDA methods that use large frequency increments [8], [17]. It requires a large frequency increment when the FDA forms an angle-range-dependent beam pattern in the short range using continuous waves without signal processing. In this section, several nonlinearly changing frequency increment methods are proposed.

A. Exponential Frequency Increment of m^{α}

One of the simplest methods to make a nonlinear function is the m-th power. The frequency increment is derived as follows:

$$\Delta f_m = m^{\alpha}\Delta f\,, \tag{24}$$

where α is a control parameter for the AF. Using (4) and (24), the accurate meaning of time (t) [25], the AF in this case is derived as

$$AF(t,R,\theta) = \sum_{m=0}^{M-1} u\left(t-\frac{R}{c}\right) e^{j2\pi m\left[m^{\alpha-1}\Delta f\left(t-\frac{R}{c}\right)+\frac{f_0 d\sin\theta}{c}\right]+\mathrm{j}\varphi_m} \tag{25}$$

where the function $u(t)$ is the unit step function expressed in (26).

$$u(t) = \begin{cases} 1, & t \geq 0 \\ 0, & t < 0 \end{cases} \tag{26}$$

Equation (26) is an important function for explaining the relationship between time and range because the AF of FDA is a function of time (t), range (R), and angle (θ). Equation (25) is a range-dependent beam pattern because both time (t) and range (R) are variables. It should be noted that (25) remains a range-dependent pattern, although $t = R/c$ because R is a variable. It has an angle-range-dependent property in every case. The phase offset is assigned with (27) or (28) to focus the EM energy at (R_0, θ_0) at the desired time.

$$\varphi_m = \frac{2\pi m^{\alpha}\Delta f R_0}{c} - \frac{2\pi f_0 m d\sin\theta_0}{c} \tag{27}$$

$$\varphi_m = -\left(\frac{2\pi m^{\alpha}\Delta f R_0}{c} + \frac{2\pi f_0 m d\sin\theta_0}{c}\right) \tag{28}$$

It should be noted that (27) is valid for a periodic case, and (28) is valid for the non-periodic case to control the time to reach (R_0, θ_0).

The AF of the FDA is modified using (25), (27), and (28):

$$AF(t,R,\theta) = \sum_{m=0}^{M-1} u\left(t-\frac{R}{c}\right) e^{j2\pi m\left[m^{\alpha-1}\Delta f\left(t-\frac{R\pm R_0}{c}\right)+\frac{f_0 d(\sin\theta-\sin\theta_0)}{c}\right]} \tag{29}$$

There are three degrees of freedom, namely, $m, \alpha,$ and Δf, to design the FDA. For example, the AF of the FDA is not a period function when α is not an integer.

This frequency increment has two maximum points in a periodic range when α is an integer. This can be explained by the property of the frequency difference discussed in Section III. When $f_0 d(\sin\theta - \sin\theta_0)/c = 1$ and $t - (R \pm R_0)/c = 1/\Delta f$, (29) can be simplified as

$$AF(t,R) = \sum_{m=0}^{M-1} u\left(t-\frac{R}{c}\right) e^{j2\pi m[m^{\alpha-1}+1]} \tag{30}$$

Equation (29) provides the maximum point when $t \geq R/c$. This property indicates that the phase offset of the angle-element term can change the number of maximum points of the AF. This is because the common maximum point is existed when $\sin\theta = \sin\theta_0$ and $t = (R \pm R_0)/c$. This means (30) makes another maximum case when α is an integer number. Using this method, the number of maximum points in one period and the period of the FDA system can be chosen. It should be noted that the log-FDA has a single maximum point while the linear-FDA has infinite number of maximum points. The phase of two different maximum points in one period can be manipulated simultaneously by adjusting φ_m. This is the main difference compared to the reported research efforts.

B. Exponential Frequency Increment of β^m

Similar to *the* m^{α} frequency increment method, this method results in either high or low SDFI values. In this study, m was set as an integer number.

The frequency increment is expressed as

$$\Delta f_m = \beta^m \Delta f \tag{31}$$

where β is a variable. At the desired time, the phase offset is assigned as (32) to form a maximum point at (R_0, θ_0)

$$\varphi_m = \pm\frac{2\pi\beta^m\Delta f R_0}{c} - \frac{2\pi f_0 m d\sin\theta_0}{c} \tag{32}$$

The sign of φ_m determines the period of AF: a positive sign for periodic AF and a negative sign for a non-periodic function. Using the same method applied in the previous section, the AF is derived as

$$AF(t,R,\theta) = \sum_{m=0}^{M-1} u\left(t-\frac{R}{c}\right) e^{j2\pi\left[\beta^m\Delta f\left(t-\frac{R\pm R_0}{c}\right)+\frac{2\pi m f_0 d(\sin\theta-\sin\theta_0)}{c}\right]} \tag{33}$$

V. Case Study and Experimental Results

A. AF Analysis Using Periodicity and Accurate Time

The time term should be thoroughly analyzed to realize the FDA system. The key design parameters of the FDA methods for analysis are listed in Table I. In this study, the EM energy is focused at ($5m$, 40°) using the FDA method with phase offset

TABLE I. KEY DESIGN PARAMETERS OF FDA: GCD, PERIODICITY, AND FREQUENCY INCREMENT METHODS

FDA Type	Log-FDA	Linear	2^m	m^2	1.5^m	$m^{1.5}$
Frequency increment (M = 9)	$\Delta f_m = 3\log(m+1)\,10^8$	$\Delta f_m = 3.3\times10^7\times m$	$\Delta f_m = 5.9\times10^5\times2^m$	$\Delta f_m = \frac{1.1}{3}\times10^7\times m^2$	$\Delta f_m = 7.7\times10^6\times(1.5)^m$	$\Delta f_m = 1.1\times10^7\times m^{1.5}$
GCD	X	3.3×10^7	5.9×10^5	X	X	X
Periodicity [s]	X	$\frac{1}{3.3}\times10^{-7}$	$\frac{1}{5.9}\times10^{-5}$	$\frac{3}{1.1}\times10^{-7}$	2×10^3	X
Maximum Frequency (MHz)	300	297	297	297	296	297
Center Frequency (GHz)	24	24	24	24	24	24

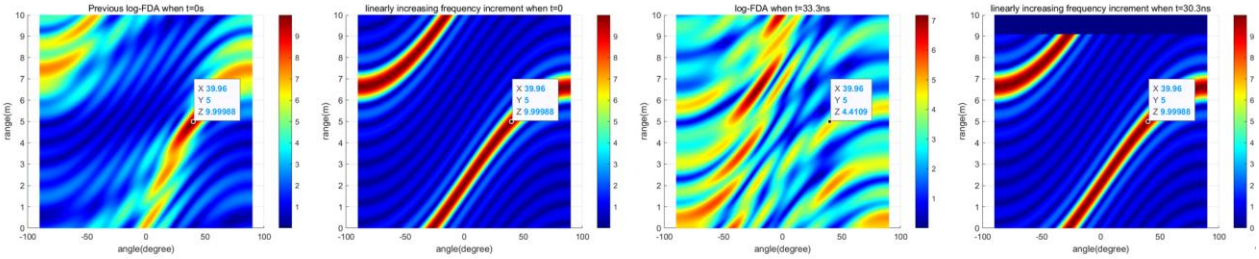

(a) (b) (c) (d)

Fig. 4. AFs in angle-range dimensions: (a) log-FDA at t = 0, (b) linear FDA at t = 0, (c) log-FDA at t = 33.3 ns, and (d) linear FDA at t = 30.3 ns.

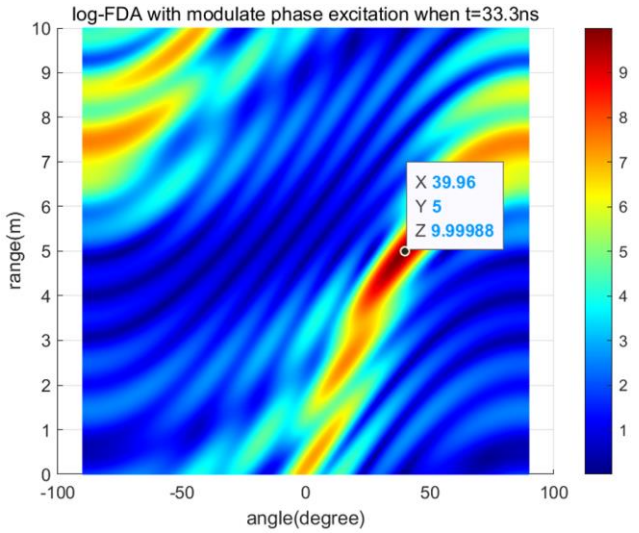

Fig. 5. AF of log-FDA with phase offset values related to range-time-frequency term.

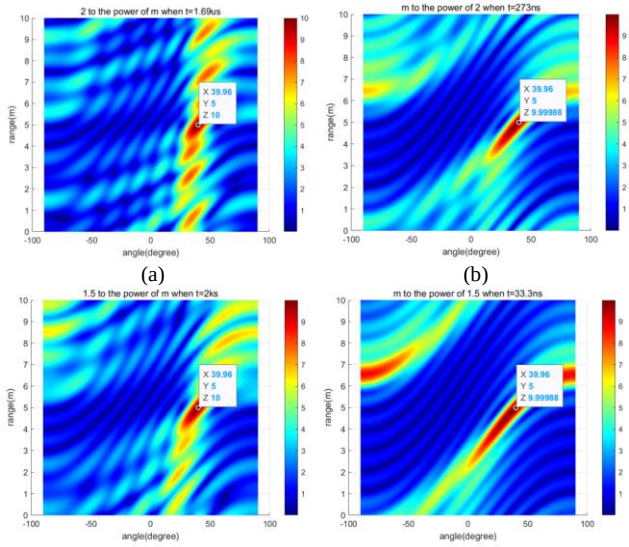

(a) (b) (c) (d)

Fig. 6. AFs of the proposed exponential-FDA methods shown in Table I: (a) 2^m, (b) m^2, (c) 1.5^m, and (d) $m^{1.5}$.

values presented in (12), (27), and (31). Fig. 4 shows both the log-FDA and linearly increasing frequency increment methods. Figs. 4(a) and (b) show two frequency increment methods when the speed of the EM wave is neglected, while the AFs presented in Figs. 4(c) and (d) depict the beam patterns of log and linear FDA methods, respectively, with the proposed time principal.

Fig. 4(c) does not have a maximum point in the given range because of the phase offset related to the range-time-frequency term. Equation (20) should be considered to focus EM energy at the desired location, as shown in Fig. 4(a). Fig. 5 shows the focused EM energy at the desired location using the log-FDA method when t = 33.3 ns. The phase offset related to the range-time-frequency term makes a maximum point at (R, 40°), when $t = (R+R_0)/c$, according to (21). This validates the meaning of the phase offset, which controls the arrival time of the beam and the angle of the maximum point. Time and phase offset should be considered simultaneously when manipulating the location of the maximum point of the FDA. Furthermore, the phase offset should be thoroughly considered according to the presence of periodicity because different phase offset methods should be applied depending on its periodicity. The blank part shown in Fig. 4(d) is the area, where the EM wave has not yet been reached.

The beam patterns of the proposed exponential-FDA method with an accurate time analysis are shown in Fig. 6. It shows

TABLE II. SDFI VALUES OF FDAS

Frequency increment method	Number of elements (M)	SDFI	Maximum frequency difference (MHz)	M_D	80% power area (%)
Log-FDA	10	0.408	297	9	0.571
2^m-FDA	10	0.933	297	6	0.279
m^2-FDA	10	0.335	297	9	0.589
m^2-FDA	10	1.674	1490	9	0.118
1.5^m-FDA	10	0.536	297	9	0.395
$m^{1.5}$-FDA	10	0.204	297	9	1.081
Random-log FDA [15]	10	2.488	297	9	0.170
Random-linear FDA [15]	10	2.719	297	9	0.164
Multi carrier log-FDA [6]	10	1.256	298	9	0.151

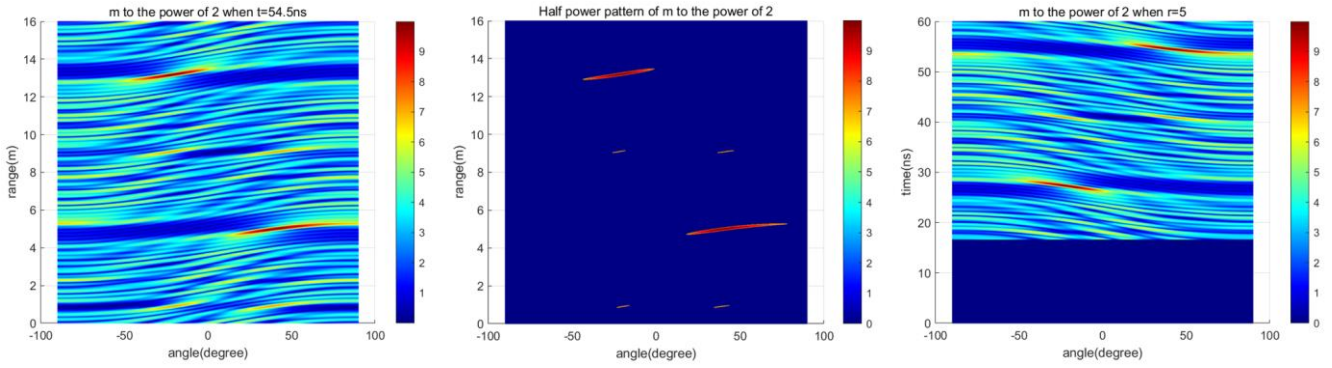

(a) (b) (c)

Fig. 7. AF of m^2: (a) angle-range dimension beam pattern, (b) half power beam pattern in angle-range dimensions, and (c) time-angle dimension beam pattern at $R = 5m$.

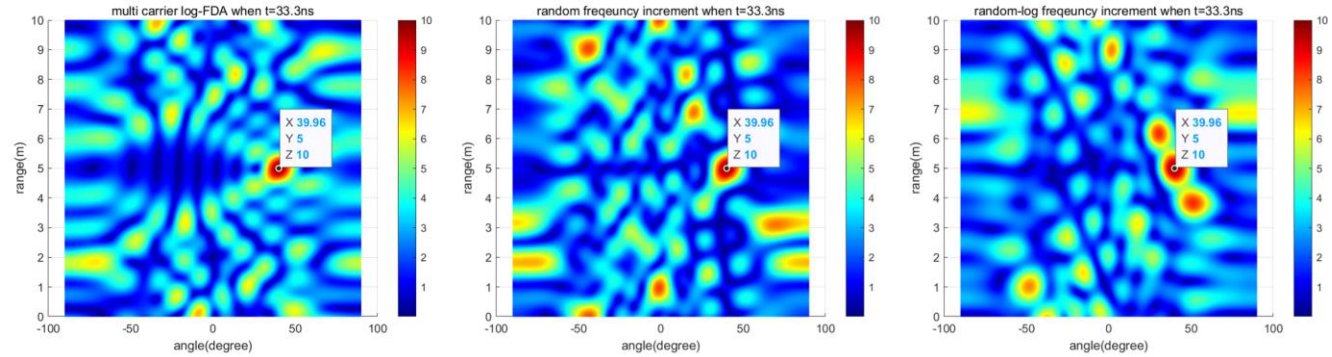

(a) (b) (c)

Fig. 8. AF of FDAs: (a) multi carrier log-FDA (3 carriers [6]), (b) random linear FDA [15], and (c) random-log FDA [15].

periodicity, as presented in Table I. However, the AF shown in Fig. 6(d) does not have periodicity and requires accurate time analysis proposed in (33) to focus EM energy at the desired position.

B. FDA Analysis by Using SDFI

The SDFI is proposed to analyze the frequency increment methods. Table II lists the properties of several frequency increment method examples. The area of the spot where 80% of the radiated power is concentrated is presented to demonstrate the proposed SDFI FDA analysis method. The RF power of a given area is calculated as dividing power of specific position by theoretical maximum power of FDA, $|AF(t,R,\theta)|^2/m^2$. The area of focused RF power is divided by the whole area of interest. It is adapted to represent the density of maximum point. In this study, the range is $10m$ and the power is 80%.

It is clear that $m^{1.5}$-FDA has the lowest SDFI value, while random-linear FDA has the highest SDFI value. The 2^m-FDA has $M_D = 6$. This indicates that this system has a higher tendency to have a beam pattern of a phased array. The proposed SDFI analysis method discussed in Section III successfully explains 80% of the power areas shown in Fig. 6 and 8.

Two similar m^2-FDA methods are also analyzed to validate the SDFI method. The quotients of the SDFI, 80% power area, and maximum frequency difference between these two methods are almost the same. This shows that the proposed SDFI method is useful for comparing FDA methods with the same frequency

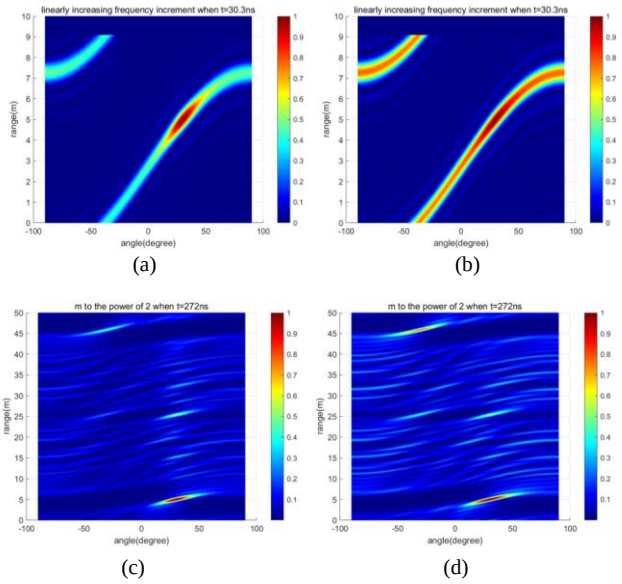

Fig. 9. Effects of antenna coupling on FDA: linear FDA (a) with S_{iso} = 20 dB, (b) S_{iso} = 30 dB, and m^2 FDA (c) with S_{iso} = 20 dB, (d) S_{iso} = 30 dB.

increment method. Fig. 7(a) is clearly more affected by range than Fig. 6(b), while Fig. 7(a) has a smaller maximum area than Fig. 6(b). This implies that, when two FDA's have the same frequency increment methods, the case of a larger maximum frequency value is more affected by the range. This is because a short pulse-like beam pattern is formed when a larger maximum frequency increment is employed.

Fig. 7 shows the special property of m^{α} when α is an integer. In this study, α was set to 2 for ease of calculation. A maximum point is calculated according to (30). In Fig. 7(c), the unit step function shown in (26) guarantees the causality of the proposed FDA theory, and it shows when energy is first transferred to specific range at $R = 5m$. It is noteworthy that the calculated maximum point can be manipulated by the phase offset values at any angle. Beam patterns (AFs) of the reported FDA theories are reproduced based on the proposed FDA analysis method as shown in Fig. 8 for the comparison. These figures have dot-shaped form because of co-existence of increasing and decreasing frequency steps. These shapes are easily predicted by high SDFI value.

C. Effects of Antenna Coupling on FDA

The effects of coupling occurred among the antenna elements of the FDA system should be analyzed because each antenna element radiates EM waves at different frequencies and generates phase offsets. The *S*-parameter of the FDA antenna array (S^{FDA}) consisting of M antenna elements is an $M \times M$ symmetric matrix, which is decomposed into two parts: (1) antenna matrix (S^A) and (2) coupling (or isolation) matrix (S^C) between antenna elements.

$$S^{FDA} = S^A + S^C \tag{34}$$

where S^A is a symmetric diagonal matrix that represents the reflection coefficients of the M-antenna array without any coupling and S^C is a symmetric hollow matrix. In this case study, the AF of the FDA is re-calculated by considering the coupling level between adjacent antenna elements. In particular, all antenna elements radiate all signals fed to the antenna array using a weighting factor of the coupling (isolation) matrix.

TABLE III. FDA PROPERTIES

Ref.	Center Freq. (GHz)	Max. Freq. Step	Number of Elements	Range coverage
Fig. 7(b)	24	297 MHz	10	2.7 m
[4]	10	100 kHz	36	Not Shown
[5]	10	Not Shown	20	Not Shown
[6]	3.0	Not Shown	17	15 km
[11]	5.0	1 kHz	10	30 km
[13]	5.0	2 kHz	10	Not Shown
[14]	5.0	30 kHz	15	Not Shown
[15]	8.0	24 kHz	16	Not Shown
[15]	8.0	21 kHz	16	Not Shown
[17]	6.0	Not Shown	16	1.5 m
[20]	2.45	10 MHz	8	Not Shown
[22]	3.2	Not Shown	8	8.8 km
[22]	10	Not shown	10	16 km

Fig. 9 shows beam-pattern ($|AF(t,R,\theta)|^2$) of the linear and exponential FDA methods according to antenna coupling levels. Figs. 9 (a) and (b) show the beam patterns of linear FDA with antenna coupling level of 20 dB and 30 dB, respectively. Fig. 9 (a) shows that the linear FDA with 20 dB isolation between the antenna elements loses the auto-scanning characteristic of the linear FDA. This result demonstrates the importance of antenna coupling (or isolation) in the FDA system. Figs. 9 (c) and (d) show the m^2 FDA with finite antenna coupling level when the desired two beam focusing positions are (R, $\pm 30^{\circ}$). The isolation level between adjacent antenna elements should be higher than 30 dB to maintain a beam pattern of two peaks. It should be noted that an antenna array must be carefully designed to achieve the desired beam patterns given that antenna radiation pattern and isolation between antenna elements are critical design parameters of FDAs.

D. Case Study: FDA for WPT

In this section, a practical WPT system based on the proposed FDA theory is presented. The proposed FDA system for WPT consists of square patch antennas, as the patch antenna array has a relatively low antenna-to-antenna coupling. The patch antenna array for the FDA-based WPT system operates at 24 GHz (BW: 24.0–24.3 GHz), and the proposed exponential FDA method of m^2 frequency increment is shown in Table I. The receiver system reported in [26] was placed at 10 cm, $\pm 30^{\circ}$. Using the Friis transmission equation and the beam patterns of the proposed FDA, the transferred power to -30° is calculated as 15.7 dBm, and $+30^{\circ}$ is 14.7 dBm, if the transmitted power is 37 dBm (5 W). The transferred power to each energy harvester is 11.2 dBm and 10.2 dBm, respectively, given that the RF-to-DC conversion efficiency was 35.1 %. It should be noted that the energy harvester cannot collect EM energy when it is located other than (10 cm, $\pm 30^{\circ}$) because of periodicity of m^2-FDA shown in Table I. The periodicity is an important factor in applying the proposed FDA theory to analyze WPT systems. Otherwise, it is challenging to effectively energize the RF power harvester. The proposed FDA method enables to control the number of target points (peaks of AF in the given area). For example, there are two target points as demonstrated in Fig. 9(d). It is the main novelty of this method because the other

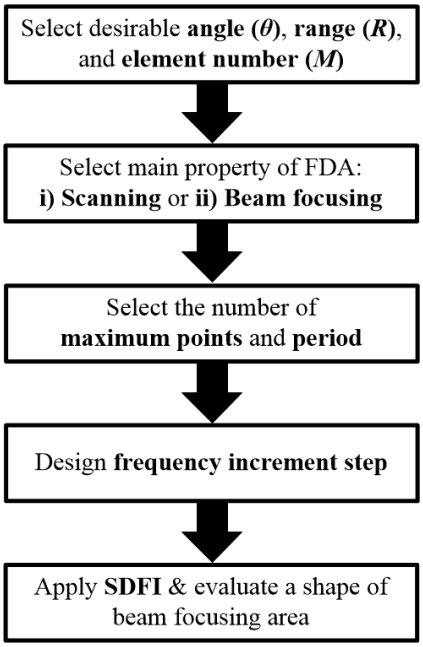

Fig. 10. Flowchart of the proposed FDA analysis and design algorithm.

FDA methods have only one peak point except linear-FDA which has a beam scanning property.

One of the most critical key performance indicators in the practical implementation of FDA is to control the phase shift of RF signal fed to the antenna array. Reported research efforts on the FDA system have demonstrated the practicality of FDA [27], [28]. The feasibility of FDA system is demonstrated using a commercial software defined radio (SDR) and oscillator ICs. The method and algorithm proposed in this paper can be scaled to any frequency band and implemented on commercial platforms. Table III summarizes the properties of the reported research efforts on FDA methods. The inverse proportion relationship between the range and frequency step is observed in Table I, as discussed in this paper. Fig. 10 shows the proposed beam synthesis flow for designing an optimized FDA under the given conditions and design targets.

VI. Conclusion

This paper presented a novel analysis and design method for FDA. The relationship between the frequency increment and time was also presented. The rate of frequency increment change provided useful information related to the AF of the FDA. Multiple maximum points and methods for controlling their locations using the proposed FDA analysis were discussed. Periodicity of the FDA and manipulation of the phase offset discussed in this study have paved a new way to analyze the FDA. Using the proposed methods, beam patterns with scanning properties (a linearly increasing frequency increment) or quasi-pulse wave properties (nonlinearly changing frequency increments) can be easily synthesized. All proposed FDA methods and analytical techniques have been demonstrated, and the calculated results were consistent with the theory developed in this study.

References

[1] P. Antonik, M. C. Wicks, H. D. Griffiths, and C. J. Baker, "Frequency diverse array radars," *2006 IEEE Conference on Radar*, Verona, NY, USA, 24-27 Apr. 2006.

[2] W. Wang, "Frequency diverse array antenna: new opportunities," *IEEE Antennas Propag. Mag.*, vol. 57, no. 2, pp. 145-152, Apr. 2015.

[3] W. Wang, "Ultrawideband frequency-diverse array antennas: range-dependent and autoscanning beampattern applications," *IEEE Antennas Propag. Mag.*, vol. 60, no. 3, pp. 48-56, Jun. 2018.

[4] A. Akkoc, E. Afacan, and E. Yazgan, "Dot-shaped 3d range-angle dependent beamforming with discular frequency diverse array," *IEEE Trans. Antennas Propag.*, Early Access, Apr. 2021.

[5] Y. Liao, J. Wang, and Q. H. Liu, "Transmit beampattern synthesis for frequency diverse array with particle swarm frequency offset optimization," *IEEE Trans. Antennas Propag.*, vol. 69, no. 2, pp. 892-901, Feb. 2021.

[6] M. Mahmood and H. Mir, "Frequency diverse array beamforming using nonuniform logarithmic frequency increments," *IEEE Antennas Wirel. Propag. Lett.*, vol. 17, no. 10, pp. 1817-1821, Oct. 2018.

[7] W. Khan and I. M. Qureshi, "Frequency diverse array radar with time-dependent frequency offset," *IEEE Antennas Wirel. Propag. Lett.*, vol. 13, pp. 758-761, Apr. 2014.

[8] A.-M. Yao, P. Rocca, W. Wu, A. Massa, and D.-G. Fang, "Synthesis of time-modulated frequency diverse arrays for short-range multi-focusing," *IEEE J. Sel. Topics Signal Process.*, vol. 11, no. 2, pp. 282-294, Mar. 2017.

[9] A.-M. Yao, W. Wu, and D.-G. Fang, "Frequency diverse array antenna using time-modulated optimized frequency offset to obtain time invariant spatial fine focusing beampattern," *IEEE Trans. Antennas Propag. Lett.*, vol. 64, no. 10, pp. 4434-4446, Oct. 2016.

[10] K. Chen, S. Yang, Y. Chen, and S.-W. Qu, "Accurate models of time-invariant beampatterns for frequency diverse arrays," *IEEE Trans. Antennas Propag.*, vol. 67, no. 5, pp. 3022-3029, May 2019.

[11] B. Chen, X. Chen, Y. Huang, and J. Guan, "Transmit beampattern synthesis for the fda radar," *IEEE Antennas Wirel. Propag. Lett.*, vol. 17, no. 1, pp. 98-101, Jan. 2018.

[12] M. Secmen, S. Demir, A. Hizal and T. Eker, "Frequency diverse array antenna with periodic time modulated pattern in range and angle," *2007 IEEE Radar Conference*, Waltham, MA, USA, 17-20 Apr. 2007, pp. 427-430.

[13] W. Khan, I. M. Qureshi, and S. Saeed, "Frequency diverse array radar with logarithmically increasing frequency offset," *IEEE Antennas Wirel. Propag. Lett.*, vol. 14, pp. 499-502, Nov. 2015.

[14] L. Zhang, W. Xu, P. Huang, and W. Tan, "Comparison of frequency diverse array patterns with nonuniform frequency offset," *2020 IEEE MTT-S International Wireless Symposium (IWS)*, Shanghai, China, 20-23 Sep. 2020.

[15] G. Huang, Y. Ding, S. Ouyang, and V. Fusco, "Frequency diverse array with random logarithmically increasing frequency offset," *Microw. Opt. Technol. Lett.*, vol. 62, no. 7, pp. 2554-2561, Feb. 2020.

[16] Y. Liu, H. Ruan, L. Wang. and A. Nehorai, "The random frequency diverse array: a new antenna structure for uncoupled direction-range indication in active sensing," *IEEE J. Sel. Topics Signal Process.*, vol. 11, no. 2, pp. 295-308, Mar. 2017.

[17] Z. Wang, Y. Song, T. Mu, and Z. Ahmad, "A short-range range-angle dependent beampattern synthesis by frequency diverse array," *IEEE Access*, vol. 6, pp. 22664-22669, 2018.

[18] W. Wang, "DM using fda antenna for secure transmission," *IET Microw., Antennas Propag.*, vol. 11, no. 3, pp. 336–345, Dec. 2016.

[19] S. Ji, W. Wang, H. Chen and Z. Zheng, "Secrecy capacity analysis of an-aided fda Communication Over nakagami-m Fading," *IEEE Wireless Commun. Lett.*, vol. 7, no. 6, pp. 1034-1037, Dec. 2018.

[20] E. Fazzini, M. Shanawani, A. Costanzo, and D. Masotti, "A logarithmic frequency-diverse array system for precise wireless power transfer," *2020 50th European Microwave Conference (EuMC)*, Utrecht, Netherlands, 12-14 Jan. 2021, pp. 646-649.

[21] C. A. Balanis, *Antenna Theory Analysis and Design*. 4nded., New Jersey, USA: A John Wiley & Sons inc., 2016, pp. 286-287.

[22] C. Cui, W. Li, X. Ye, Y. Hei, and X. Shi, "A short-time range-angle-decoupled beam pattern synthesis for frequency diverse arrays," *IET Microw. Antennas Propag. Lett.*, vol. 15, pp. 855-870, Mar. 2021.

[23] R. J. Mailloux, "Phased array theory and technology," *Proc. IEEE*, vol. 70, no. 3, pp. 246-291, Mar. 1982.

[24] J. L. Cruz, B. Ortega, M. V. Andres, B. Gimeno, J. Capmany, and L. Dong, "Array factor of a phased array antenna Steered by a chirped fiber grating beamformer," *IEEE Photonics Technol. Lett.*, vol. 10, no. 8, pp. 1153-1155, Aug. 1998.

[25] M. Tan, C. Wang, and Z. Li, "Correction analysis of frequency diverse array radar about time," *IEEE Trans. Antennas Propag.*, vol. 69, no. 2, pp. 834-847, Feb. 2021.

[26] S. Daskalakis, J. Kimionis, J. Hester, A. Collado, M. M. Tentzeris and A. Georgiadis, "Inkjet printed 24 GHz rectenna on paper for millimeter wave identification and wireless power transfer applications," *2017 IEEE MTT-S Int. Microw. Workshop Series on Advanced Materials and Processes for RF and THz Applications (IMWS-AMP)*, Pavia, Italy, 20-22 Sep. 2017.

[27] T. Eker, S. Demir, and A. Hizal, "Exploitation of linear frequency modulated continuous waveform (LFMCW) for frequency diverse arrays," *IEEE Trans. Antennas Propag.*, vol. 61, no. 7, pp. 3546-3553, Jul. 2013.

[28] E. Fazzini, A. Costanzo and D. Masotti, "Range Selective Power Focusing with Time-controlled Bi-dimensional Frequency Diverse Arrays," *2021 IEEE Wireless Power Transfer Conference (WPTC)*, San Diego, CA, USA, 1-4 Jun. 2021.

Woohyeok Choi received the B.S. degree from the Department of Electronics Engineering, Pusan National University, Busan, South Korea, in 2021. His research interests include AI-assisted RF system and array antenna.

Apostolos Georgiadis (Fellow, IEEE) was born in Thessaloniki, Greece. He received the B.S. degree in physics and the M.S. degree in telecommunications from the Aristotle University of Thessaloniki, Greece, in 1993 and 1996, respectively, and the Ph.D. degree in electrical engineering from the University of Massachusetts, Amherst, MA, USA, in 2002. In 2002, he joined Global Communications Devices (GCD), North Andover, MA, USA, as a Systems Engineer and worked on CMOS transceivers for wireless network applications. In June 2003, he joined Bermai, Inc., Minnetonka, MN, USA, as an RF/Analog Systems Architect. In 2005, he joined the University of Cantabria, Santander, Spain, as a Juan de la Cierva Fellow. In March 2007, he joined CTTC, Barcelona, Spain, as a Senior Research Associate in the area of communications subsystems. From 2013 to 2016, he was a Group Leader with the Microwave Systems and Nanotechnology Department, CTTC. In July 2016, he joined Heriot-Watt University, Edinburgh, U.K., as an Associate Professor. Since 2017, he has been with the European Patent Office, The Hague, Netherlands. He has published more than 200 articles in peer reviewed journals and international conferences. His research interests include energy harvesting and wireless power transmission, radio frequency identification (RFID) technology, active antennas and phased array antennas, inkjet and 3-D printed electronics, millimeter wave systems. Dr. Georgiadis is an EU Marie Curie Global Fellow and URSI Fellow. He was a recipient of the 2016 Bell Labs Prize (Third Place). He was the General Chair of 2011 IEEE RFID-TA Conference and the General Co-Chair of the 2011 IEEE MTT-S IMWS on Millimeter Wave Integration Technologies. He was the Chair of URSI Commission D: Electronics and Photonics. He has been an Associate Editor for the IEEE Journal on Radio Frequency Identification, the IEEE Microwave and Wireless Components Letters, the IET Microwaves Antennas and Propagation, and the IEEE Radio Frequency Identification Virtual Journal. He co-founded and was an Editor-in-Chief of the Cambridge Wireless Power Transfer Journal. He has been a Distinguished Lecturer of IEEE CRFID.

Manos M. Tentzeris (S'89–M'92–SM'03–F'10) received the Diploma degree (magna cum laude) in electrical and computer engineering from the National Technical University of Athens, Athens, Greece, and the M.S. and Ph.D. degrees in electrical engineering and computer science from the University of Michigan, Ann Arbor, MI, USA. He is currently Ken Byers Professor in flexible electronics with the School of Electrical and Computer Engineering, Georgia Institute of Technology, Atlanta, GA, USA, where he heads the ATHENA Research Group (20 researchers). He has served as the Head of the GTECE Electromagnetics Technical Interest Group, as the Georgia Electronic Design Center Associate Director of RFID/Sensors research, as the Georgia Institute of Technology NSF-Packaging Research Center Associate Director of RF Research, and as the RF Alliance Leader. He has helped develop academic programs in 3-D/inkjet-printed RF electronics and modules, flexible electronics, origami and morphing electromagnetics, highly integrated/multilayer packaging for RF, millimeter-wave, sub-THz and wireless applications using ceramic and organic flexible materials, paper-based RFID's and sensors, wireless sensors and biosensors, wearable electronics, "Green" electronics, energy harvesting and wireless power transfer, nanotechnology applications in RF, microwave MEMs, and SOP-integrated (UWB, multiband, mmW, and conformal) antennas. He has authored more than 850 papers in refereed journals and conference proceedings, 7 books, and 26 book chapters. He was a Visiting Professor with the Technical University of Munich, Munich, Germany, in 2002, with GTRI-Ireland, Athlone, Ireland, in 2009, and with LAAS-CNRS, Toulouse, France, in 2010. Dr. Tentzeris was a recipient/co-recipient of the 2022 Georgia Tech Outstanding Doctoral Thesis Advisor Award, the 2019 Humboldt Research Prize, the 2017 Georgia Institute of Technology Outstanding Achievement in Research Program Development Award, the 2016 Bell Labs Award Competition 3rd Prize, the 2015 IET Microwaves, Antennas, and Propagation Premium Award, the 2014 Georgia Institute of Technology ECE Distinguished Faculty Achievement Award, the 2014 IEEE RFID-TA Best Student Paper Award, the 2013 IET Microwaves, Antennas and Propagation Premium Award, the 2012 FiDiPro Award in Finland, the iCMG Architecture Award of Excellence, the 2010 IEEE Antennas and Propagation Society Piergiorgio L. E. Uslenghi Letters Prize Paper Award, the 2011 International Workshop on Structural Health Monitoring Best Student Paper Award, the 2010 Georgia Institute of Technology Senior Faculty Outstanding Undergraduate Research Mentor Award, the 2009 IEEE TRANSACTIONS ON COMPONENTS AND PACKAGING TECHNOLOGIES Best Paper Award, the 2009 E. T. S. Walton Award from the Irish Science Foundation, the 2007 IEEE AP-S Symposium Best Student Paper Award, the 2007 IEEE MTT-S IMS Third Best Student Paper Award, the 2007 ISAP 2007 Poster Presentation Award, the 2006 IEEE MTT-S Outstanding Young Engineer Award, the 2006 Asia– Pacific Microwave Conference Award, the 2004 IEEE TRANSACTIONS ON ADVANCED PACKAGING Commendable Paper Award, the 2003 NASA Godfrey "Art" Anzic Collaborative Distinguished Publication Award, the 2003 IBC International Educator of the Year Award, the 2003 IEEE CPMT Outstanding Young Engineer Award, the 2002 International Conference on Microwave and Millimeter-Wave Technology Best Paper Award (Beijing, China), the 2002 Georgia Institute of Technology–ECE Outstanding Junior Faculty Award, the 2001 ACES Conference Best Paper Award, the 2000 NSF CAREER Award, and the 1997 Best Paper Award of the International Hybrid Microelectronics and Packaging Society. He was the TPC Chair of the IEEE MTT-S IMS 2008 Symposium and the Chair of the 2005 IEEE CEM-TD Workshop. He is the Vice-Chair of the RF Technical Committee (TC16) of the IEEE CPMT Society. He is the Founder and Chair of the RFID Technical Committee (TC24) of the IEEE MTT-S and the Secretary/Treasurer of the IEEE C-RFID. He is an Associate Editor of the IEEE TRANSACTIONS ON MICROWAVE THEORY AND TECHNIQUES, the IEEE TRANSACTIONS ON ADVANCED PACKAGING, and the International Journal on Antennas and Propagation. He has given more than 100 invited talks to various universities and companies all over the world. He is a member of the URSI-Commission D and the MTT-15 Committee, an Associate Member of EuMA, a Fellow of the Electromagnetic Academy, and a member of the Technical Chamber of Greece. He served as one of the IEEE MTT-S Distinguished Microwave Lecturers from 2010 to 2012 and is one of the IEEE CRFID Distinguished Lecturers.

Sangkil Kim (M'15-SM'20) received his B.S. degree from School of Electrical and Electronics Engineering, Yonsei University (magna cum laude), Seoul, Republic of Korea in 2010. He received his M.S. and Ph.D. degrees from School of Electrical and Computer Engineering, Georgia Institute of Technology, GA, Atlanta, USA in 2012 and 2014, respectively. From 2015 to 2018, he worked at Qualcomm, inc., San Diego, CA, USA as a senior engineer. He joined the faculty of Department of Electronics Engineering, Pusan National University, Busan, Republic of Korea in 2018. He has published 44 papers in peer reviewed journals and 5 book chapters. Dr. Kim received the IET Premium Award Microwave, Antennas & Propagation in 2015 and KIEES Young Researcher Award in 2019. He is a member of the IEEE MTT-26 RFID, Wireless Sensors, and IoT Committee. His main research interests are mmWave phased antenna array, machine learning assisted backscattering communication, RF biosensors, energy harvesting and printed RF electronics.